NASA TN D-1565

TECHNICAL NOTE

D-1565

EXPERIMENTAL EVALUATION OF THEORETICAL ELASTIC STRESS DISTRIBUTIONS FOR CYLINDER-TO-HEMISPHERE AND CONE-TO-SPHERE JUNCTIONS IN PRESSURIZED SHELL STRUCTURES

By William C. Morgan and Peter T. Bizon

Lewis Research Center
Cleveland, Ohio

NATIONAL AERONAUTICS AND SPACE ADMINISTRATION
WASHINGTON
February 1963

Copy 1

Code 1

NATIONAL AERONAUTICS AND SPACE ADMINISTRATION

TECHNICAL NOTE D-1565

EXPERIMENTAL EVALUATION OF THEORETICAL ELASTIC STRESS DISTRIBUTIONS FOR CYLINDER-TO-HEMISPHERE AND CONE-TO-SPHERE JUNCTIONS IN PRESSURIZED SHELL STRUCTURES

By William C. Morgan and Peter T. Bizon

SUMMARY

The elastic stress distributions of two shell junctions that have application in space-vehicle design were measured. The junctions were a cylinder with a hemisphere and a cone with a portion of a sphere. These junctions were incorporated in a single type of structure, a cylinder with a toriconical head. Two test structures were used; the principal difference between them was the accuracy of methods used in fabrication.

The investigation was conducted to evaluate previously published analyses for determining stress distributions at these junctions under internal pressure. The data obtained from the tests were compared with theoretical curves determined from these analyses.

The general trends of the data were consistent with the theoretical stress distributions. In the spun structure, the average magnitude of percent variation of experimental stress from theoretical stress values was 9.2; the other structure, made to more exact specifications, had a variation of 3.8 percent. The principal source of experimental error appeared to be variation in geometry from the dimensional values assumed for purposes of analysis.

Evaluation of the stress distributions indicated that the half-angle of the cone was not an important parameter. It also was noted that maximum effective stress in this type of structure would be approximately $3\frac{1}{2}$ percent higher than the cylinder-membrane effective stress at any ratio of cylinder radius to wall thickness.

INTRODUCTION

An experimental investigation was made to determine the elastic stress distributions for two shell junctions that may have application in the design of

space-vehicle structures subject to internal pressure. The two junctions are:

(1) Cylinder with hemisphere

(2) Cone with portion of sphere

The purpose of the investigation was to verify analytical methods and to determine the degree of correlation between theoretical and experimental stresses in actual structures fabricated to different degrees of geometrical accuracy. The analyses used to determine theoretical stresses were obtained from a recent study of stress distributions in regions of geometrical discontinuity in shell-type structures (ref. 1).

In the test program, the two junctions were incorporated in a single type of pressure vessel, a cylinder with a toriconical head, referred to in this report as a toriconical structure. The spherical portion had the same radius as the cylindrical part of the structure and was tangent to the cone. The meridional distance between the two junctions in the structure was sufficient to eliminate any appreciable interaction.

Two toriconical structures were used in the tests. The larger structure had a nominal ratio of cylinder radius to wall thickness of 118; the smaller of the two structures had a ratio of 100. The larger structure was made by spinning and was dimensionally less accurate than the smaller one made by contour machining.

These structures were considered representative of the range of quality that might be expected for the fabrication of shell structures. It was believed that the experimental results would provide information on the qualitative significance of stresses attributable to inaccuracies in fabrication.

Data obtained from bonded electrical-resistance foil gages were used for calculation of the experimental stresses. The structures were tested under internal hydrostatic pressure, and the stresses were within the elastic range of the material even where inaccuracies in fabrication caused local stresses to be somewhat higher than those predicted by the theoretical analyses.

ANALYTICAL METHODS

Analysis for the junction of the cylinder and the portion of a sphere with the same radius as the cylinder is the same as for the junction between a cylinder and a hemisphere. This problem is considered in references 1 and 2, and the stress distribution for this junction was calculated on the basis of the procedures in these reports. The theoretical stress distribution for the junction between the cone and portion of a sphere was determined by methods given in reference 1.

The forces acting upon the two junctions are shown in figure 1. Definitions of symbols are given in appendix A, and a detailed discussion of the analyses appears in appendixes B and C together with the equations used to determine the

theoretical stress distribution for the experimental toriconical structures under internal pressure.

EXPERIMENTAL EQUIPMENT AND PROCEDURE

The larger of the two toriconical structures is shown in figure 2(a). The cone half-angle was 45°, and the nominal mean diameter of the cylindrical section was $29\frac{3}{8}$ inches. The wall thickness was 0.125±0.005 inch. The toriconical head, including a cylindrical section 2 inches in length and formed tangent to the spherical portion, was spun from 6061-O aluminum sheet. A rolled cylinder of the same material was attached to the spun head by a circumferential weld. This weld and the longitudinal seam weld in the cylinder were finished flush. The flange required for installation of the structure in the test facility was welded to the cylinder, and the complete assembly was solution-treated and aged to the T6 condition.

Figure 2(b) shows the geometry of the small toriconical structure. The cone half-angle was the same as for the larger structure, and the mean diameter was 11.94 inches. The wall thickness was 0.060±0.005 inch. The structure was formed by contour-machining from a billet of 6061-T6 aluminum. This method of fabrication is inherently more accurate than spinning, and a comparison between the two test structures indicated that the machined structure conformed more closely to the conditions that were assumed to exist for purposes of the theoretical analysis.

The meridional locations of strain measurements are shown in figures 3(a) for the spun structure and 3(b) for the machined structure. Two strain gages were mounted at each of these locations as close to the same meridion as the physical size of the gases would permit. One was oriented meridionally, the other circumferentially, for both the inner and outer surfaces.

For the spun structure, strain gages for the interior surface were mounted first. Radiographs then were made that showed gage locations with reference to triangular lead foil markers attached to the outer surface. These radiographs were used as templates for the location of the gages on the exterior surface. The markers were removed after the installation of the gages was complete.

This procedure was not necessary for locating gages on the machined structure. The interior and exterior templates used in the contour-machining were available, and accurate locations could be determined from these templates.

The gages were 120-ohm electrical-resistance bonded foil strain gages mounted with cyanoacrylate cement. Figure 4 shows a detail of the gage installation on the large structure. These gages had a strain-sensitive length of 1/8 inch. The installation on the small structure was similar in appearance with the exception that gages with elements 1/16 inch in length were used.

The spun toriconical structure installed in the test facility is shown in figure 5. Details of the end closure for the machined structure appear in figure 6. The method of bringing out the lead wires from strain gages on the interior surface was the same for both structures.

The strain-gage lead wires were brought to a terminal box near the facility and connected through a five-wire system to a multichannel digital strain recorder in an adjacent control room. This equipment, used for balancing, calibrating, controlling, scanning, and recording strain-gage output, was accurate to ±1.0 percent of the strain-gage output. The output was recorded automatically on both a typed record and a punched paper tape.

A hydraulic system supplied internal pressure to the test structures. The pressure gages used in the experiment were calibrated and found to have a maximum error of less than 0.5 pound per square inch. The test procedure consisted of raising the internal pressure to a predetermined value and returning to zero pressure. The basic cycle was repeated for progressively higher pressures. Successive increases in pressure were made in order to provide data for the correction of nonlinearities. Data were recorded at every pressure level. The data were obtained for the larger structure at pressures of 100, 110, 120, 130, 140, and 150 pounds per square inch and for the smaller toriconical structure at 200, 210, 220, 230, 240, and 250 pounds per square inch.

A computer program was used for data reduction. This program read in data from duplicate tests, corrected for zero drift, corrected for nonlinearity by using the method of least squares, averaged strains from the two tests, and converted these strains to stresses.

RESULTS AND DISCUSSION

The experimental results were compared with the theoretical stress distributions for the maximum test pressures, 150 pounds per square inch for the large toriconical structure made by spinning, and 250 pounds per square inch for the small machined structure.

Figure 7(a) presents the results obtained for the spun toriconical structure together with the curves of theoretical stress distribution. The general trends of the experimental stresses were consistent with the theoretical curves although there were considerable quantitative disparities in some locations. The average magnitude of percent variation of experimental from theoretical stresses was 9.2.

The comparison between experimental and theoretical principal stress distributions for the machined toriconical structure is shown in figure 7(b). In general, correlation was good within reasonable limits of experimental error, with an average magnitude of 3.8 percent variation of experimental from theoretical stresses. Comparison of the data and the theoretical curves showed sufficient agreement to provide the necessary verification of the analyses for the two junctions.

The comparisons shown in figure 7 were for stresses in the principal directions. Another evaluation can be made on the basis of effective stress for the purpose of comparison with the uniaxial strength of the material determined from tensile specimens. The maximum-distortion-energy theory was used to calculate the effective stresses, both theoretical and experimental:

$$\sigma_e = \sqrt{\sigma_\xi^2 + \sigma_\theta^2 - \sigma_\xi \sigma_\theta}$$

The effective stresses for the spun toriconical structure are shown in figure 8(a). Correlation near the junction between the cone and the portion of a sphere was better for the inner surface than for the outer surface, although the trends of the data were in accordance with theory. For the junction between the portion of a sphere and the cylinder, correlation was fair in the spherical portion but agreement was not good for the cylindrical part of the structure.

Figure 8(b) shows the effective stresses for the machined toriconical structure. Correlation was good, in general, with only minor disparities between data and theoretical curves of stress distribution.

Although the results obtained from the test of the spun toriconical structure tended to corroborate the theoretical methods for finding stress distributions, there was sufficient lack of agreement to indicate the presence of extraneous factors. It did not appear that the apparent errors could be attributed to the strain gages, and it was considered that inaccuracies in the actual structure were the most probable causes.

Ultrasonic measurements showed that variation in wall thickness of the spun structure was of approximately the same magnitude as that of the machined toriconical structure. Comparisons between the geometrical shapes assumed for analyses and the actual structures showed that there were appreciable variations in the case of the spun structure. These variations are shown in figure 9. This figure indicates that abrupt changes in geometry existed in the regions immediately adjacent to the junctions. The machined structure was nearly perfect in geometry; the contour was within ±0.002 inch of the true shape. On the basis of these comparisons, it was considered probable that deviation from geometry was the principal source of error in the experimental investigation and more important than variation in wall thickness.

In figure 8 the maximum theoretical effective stress can be observed to occur near the junction between the portion of a sphere and the cylinder. This stress was 3.5 percent greater than the membrane effective stress in the cylinder. In the structures used in the investigation, the nominal ratios of cylinder radius to wall thickness, a/h, were 100 and 118. It was considered that the relation between maximum effective stress and membrane effective stress in the cylinder for a number of ratios might prove interesting. The theoretical effective stresses for radius-to-thickness ratios of 30, 100, 1000, and 10,000 are presented in figure 10.

The relation between the maximum and the cylinder-membrane effective stress near the junction of the portion of a sphere with the cylinder appeared to be nearly constant for all ratios. In the vicinity of the junction of the cone and the portion of a sphere, however, the increase in radius-to-thickness ratio was accompanied by an increase in the percentage relation between the maximum and the cylinder-membrane effective stresses. The maximum effective stress near the sphere-cylinder junction, however, was always the greater.

A similar study was made of the effect of different values of cone half-angle. This parameter was found unimportant with respect to the effect upon maximum effective stress in the structure, because the maximum value was always near the sphere-cylinder junction, shown in figure 10(d).

SUMMARY OF RESULTS

A comparison between the theoretical and experimental stress states existing in two toriconical structures gave the following results:

1. The degree of correlation between the data and the theoretical curves of stress distribution indicated that the analyses were valid. For the spun toriconical structure, the average magnitude of percent variation of experimental from theoretical stress values was 9.2; the variation for the machined structure was 3.8 percent. In both cases the general trends of the experimental stresses were consistent with the theoretical stress distributions.

2. The degree of accuracy in fabrication appeared to be an important factor with regard to lack of agreement between data and theoretical stress values. Variation in wall thickness was of the same order of magnitude for both toriconical structures, but the geometry of the spun structure varied appreciably, while the machined structure was more nearly in accordance with the shapes assumed to exist for purposes of analysis. Deviation from true geometry probably was the principal cause for observed errors.

3. In the evaluation of the stress distributions for this type of structure, the half-angle of the cone was determined to be an unimportant parameter insofar as maximum stress was concerned. In addition, the maximum effective stress in the structure was observed to be on the order of $3\frac{1}{2}$ percent greater than the cylinder-membrane effective stress, regardless of the ratio of cylinder radius to wall thickness.

Lewis Research Center
National Aeronautics and Space Administration
Cleveland, Ohio, September 28, 1962

APPENDIX A

SYMBOLS

a	mean radius of cylinder and spherical shell, in.
C_1, C_2	constants used in cone analysis and defined in appendix C
E	modulus of elasticity, psi
H	radial shear force in wall of shell acting in plane perpendicular to axis of revolution, lb/in.
h	thickness of shell wall, in.
M	bending moment in wall of shell, in.-lb/in.
m	$\sqrt[4]{12(1 - \nu^2)}$
p	uniform internal pressure, lb/sq in.
x	distance along meridian, in.
α	half-angle of cone, radians
β	$\sqrt[4]{3(1 - \nu^2)/a^2h^2}$, in.$^{-1}$
δ	edge-deflection influence coefficient
λ	$\sqrt[4]{3(1 - \nu^2)a^2/h^2}$
μ	$\sqrt[4]{12(1 - \nu^2)/h^2}$, in.$^{-1/2}$
ν	Poisson's ratio
$\Theta( )$	$e^{-( )} \cos( )$
ξ	$2\mu\sqrt{x}$
σ	normal stress, psi
$\Phi( )$	$e^{-( )}[\cos( ) + \sin( )]$
φ	angle in meridian plane of spherical torus measured from cylinder-spherical torus junction, radians

$\Psi(\ )$ $e^{-(\ )}[\cos(\ ) - \sin(\ )]$

ψ angle in meridian plane of spherical torus measured from cone-spherical torus junction, radians

$\Omega(\ )$ $e^{-(\ )} \sin(\ )$

ω edge-rotation influence coefficient

Subscripts:

c cylinder

e effective

H shear force

i inner surface

k cone

M bending moment

O origin, at junction

o outer surface

p internal pressure

s sphere

ξ meridional direction

θ circumferential direction

APPENDIX B

ANALYSIS OF STRESS NEAR JUNCTION OF CYLINDER AND PORTION OF SPHERE

The junction between a cylinder and a portion of a sphere, shown in figure 1(a), may be treated as a junction between a cylinder and a hemisphere. With constant wall thickness, the equations for shear and moment given in reference 1 may be reduced to

$$H_0 = \frac{-p}{8\beta_c} = \frac{-pa}{8\lambda_s} \tag{B1}$$

and

$$M_0 = 0 \tag{B2}$$

where the sign convention is as shown in figure 1(a).

The equations for stress in the cylinder subject to internal pressure, edge shear, and zero moment are

$$\sigma_{\xi,c} = \frac{pa}{2h} \pm \frac{6}{\beta h^2} H_0 \Omega(\beta x) \tag{B3}$$

$$\sigma_{\theta,c} = \frac{pa}{h} + \left[2\beta \frac{a}{h} \Theta(\beta x) \pm \frac{6\nu}{\beta h^2} \Omega(\beta x)\right] H_0 \tag{B4}$$

Equations for stress in the portion of a sphere adjacent to the cylinder under the same conditions of internal pressure, edge shear, and zero moment are

$$\sigma_{\xi,s} = \frac{pa}{2h} - \left[\frac{1}{h} \tan \varphi \, \Psi(\lambda\varphi) \pm \frac{6a}{\lambda h^2} \Omega(\lambda\varphi)\right] H_0 \tag{B5}$$

and

$$\sigma_{\theta,s} = \frac{pa}{2h} - \left[\frac{2\lambda}{h} \Theta(\lambda\varphi) \pm \frac{6\nu a}{\lambda h^2} \Omega(\lambda\varphi)\right] H_0 \tag{B6}$$

All distances and angles were measured from the junction (fig. 1(a)). Where double signs occur, the upper sign refers to the inner surface and the lower sign to the outer surface. Values for the functions Θ, Φ, Ψ, and Ω were obtained from references 1, 2, and 3.

APPENDIX C

ANALYSIS OF STRESS NEAR JUNCTION OF CONE AND PORTION OF SPHERE

The general equations for moment and shear in terms of influence coefficients are given in reference 1. The equations used in this present investigation are for the specific cases shown in figure 1 with a cone half-angle of 45° and are as follows:

$$H_0 = \frac{\left\{-\left[\omega_{s,H_0}\left(\delta_{k,M_0} - \delta_{s,M_0}\right) - \delta_{s,H_0}\left(\omega_{k,M_0} - \omega_{s,M_0}\right)\right]\frac{a\sqrt{2}}{4} + \left(\delta_{k,p} - \delta_{s,p}\right)\left(\omega_{k,M_0} - \omega_{s,M_0}\right) - \left(\delta_{k,M_0} - \delta_{s,M_0}\right)\left(\omega_{k,p} - \omega_{s,p}\right)\right\}p}{\left(\delta_{k,M_0} - \delta_{s,M_0}\right)\left(\omega_{k,H_0} - \omega_{s,H_0}\right) - \left(\delta_{k,H_0} - \delta_{s,H_0}\right)\left(\omega_{k,M_0} - \omega_{s,H_0}\right)} \tag{C1}$$

and

$$M_0 = \frac{\left[-\left(\delta_{s,H_0}\omega_{k,H_0} - \delta_{k,H_0}\omega_{s,H_0}\right)\frac{a\sqrt{2}}{4} + \left(\delta_{k,H_0} - \delta_{s,H_0}\right)\left(\omega_{k,p} - \omega_{s,p}\right) - \left(\delta_{k,p} - \delta_{s,p}\right)\left(\omega_{k,H_0} - \omega_{s,H_0}\right)\right]p}{\left(\delta_{k,M_0} - \delta_{s,M_0}\right)\left(\omega_{k,H_0} - \omega_{s,H_0}\right) - \left(\delta_{k,H_0} - \delta_{s,H_0}\right)\left(\omega_{k,M_0} - \omega_{s,M_0}\right)} \tag{C2}$$

Numerical values of the edge-influence coefficients were substituted into equations (C1) and (C2) to determine the discontinuity shear and moment. Expressions for the edge-influence coefficients appear in references 1 and 4 and are given as follows:

$$\left.\begin{aligned}
\omega_{k,M_0} &= -\frac{m^3}{Eh^2}\sqrt{\frac{2a}{h}}\,\Omega_1 \\
\omega_{k,H_0} &= -\frac{m^2a}{Eh^2}\frac{\sqrt{2}}{2}\,\Omega_2 \\
\omega_{k,p} &= \frac{m^2a^2}{4Eh^2}\,\Omega_2 + \frac{3(1+\nu)}{mE}\sqrt{\frac{a}{2h}}\,\Omega_1 - \frac{3a}{2Eh} \\
\delta_{k,M_0} &= \frac{m^2a}{Eh^2}\frac{\sqrt{2}}{2}\,\Omega_2 \\
\delta_{k,H_0} &= \frac{ma}{Eh}\sqrt{\frac{a}{2h}}\,\Omega_3 \\
\delta_{k,p} &= -\frac{ma^2}{4Eh}\sqrt{\frac{a}{h}}\,\Omega_3 - \frac{m^2a\sqrt{2}}{16(1-\nu)E}\,\Omega_2 + \frac{\left(1-\frac{\nu}{2}\right)a^2\sqrt{2}}{2Eh}
\end{aligned}\right\} \tag{C3}$$

where

$$\left.\begin{aligned} \Omega_1 &= \frac{\xi_0 G}{\sqrt{2}(C + 2\nu G)} \\ \Omega_2 &= \frac{-A}{C + 2\nu G} \\ \Omega_3 &= \frac{\xi_0 B - \frac{4\nu^2 G}{\xi_0}}{\sqrt{2}(C + 2\nu G)} \end{aligned}\right\} \tag{C4a}$$

and

$$\left.\begin{aligned} A &= \xi_0(\mathrm{ber}_2'\xi_0\ \mathrm{bei}_2\xi_0 - \mathrm{bei}_2'\xi_0\ \mathrm{ber}_2\xi_0) \\ B &= (\mathrm{ber}_2'\xi_0)^2 + (\mathrm{bei}_2'\xi_0)^2 \\ C &= \xi_0(\mathrm{ber}_2\xi_0\ \mathrm{ber}_2'\xi_0 + \mathrm{bei}_2\xi_0\ \mathrm{bei}_2'\xi_0) \\ G &= (\mathrm{ber}_2\xi_0)^2 + (\mathrm{bei}_2\xi_0)^2 \end{aligned}\right\} \tag{C4b}$$

Also

$$\left.\begin{aligned} \omega_{s,M_0} &= \frac{4\lambda^3}{aEh} \\ \omega_{s,H_0} &= -\frac{\sqrt{2}\lambda^2}{Eh} \\ \omega_{s,p} &= 0 \\ \delta_{s,M_0} &= \frac{\sqrt{2}\lambda^2}{Eh} \\ \delta_{s,H_0} &= -\frac{\lambda a}{Eh} \\ \delta_{s,p} &= \frac{(1 - \nu)a^2\sqrt{2}}{4Eh} \end{aligned}\right\} \tag{C5}$$

The complete stresses are given by the following equations with the use of equations (C1) and (C2) to determine the discontinuity shear and moment:

$$\sigma_{\xi,s} = \frac{pa}{2h} + \left[\frac{2\lambda}{ah}\left(\frac{1 - \tan\psi}{1 + \tan\psi}\right)\Omega(\lambda\psi) \pm \frac{6}{h^2}\Phi(\lambda\psi)\right]M_0 + \left[\frac{1}{h}\left(\frac{1 - \tan\psi}{1 + \tan\psi}\right)\Psi(\lambda\psi) \mp \frac{6a}{\lambda h^2}\Omega(\lambda\psi)\right]\left(\frac{H_0}{\sqrt{2}} - \frac{pa}{4}\right) \tag{C6}$$

$$\sigma_{\theta,s} = \frac{pa}{2h} + \left[\frac{2\lambda^2}{ah}\Psi(\lambda\psi) \pm \frac{6\nu}{h^2}\Phi(\lambda\psi)\right]M_0 - \left[\frac{2\lambda}{h}\Theta(\lambda\psi) \pm \frac{6\nu a}{\lambda h^2}\Omega(\lambda\psi)\right]\left(\frac{H_0}{\sqrt{2}} - \frac{pa}{4}\right) \tag{C7}$$

$$\sigma_{\xi,k} = \frac{1}{hx}\left\{C_1\left[\mathrm{ber}_2\xi \mp \frac{3}{m^2}(\xi\,\mathrm{bei}_2'\xi + 2\nu\,\mathrm{bei}_2\xi)\right] + C_2\left[\mathrm{bei}_2\xi \pm \frac{3}{m^2}(\xi\,\mathrm{ber}_2'\xi + 2\nu\,\mathrm{ber}_2\xi)\right]\right\} + \left[\frac{x}{h} \pm \frac{3}{2(1 - \nu)}\right]\frac{p}{2} \tag{C8}$$

$$\sigma_{\theta,k} = \frac{1}{hx}\left\{C_1\left[\frac{\xi}{2}\,\mathrm{ber}_2'\xi \mp \frac{3}{m^2}(2\,\mathrm{bei}_2\xi + \nu\xi\,\mathrm{bei}_2'\xi)\right] + C_2\left[\frac{\xi}{2}\,\mathrm{bei}_2'\xi \pm \frac{3}{m^2}(2\,\mathrm{ber}_2\xi + \nu\xi\,\mathrm{ber}_2'\xi)\right]\right\} + \left[\frac{x}{h} \pm \frac{3}{4(1 - \nu)}\right]p \tag{C9}$$

where

$$\left.\begin{aligned} C_1 &= \frac{\left(H_0x_0h\frac{\sqrt{2}}{2} - \frac{1}{4}phx_0^2\right)(\xi_0\,\mathrm{ber}_2'\xi_0 + 2\nu\,\mathrm{ber}_2\xi_0) - 2m^2x_0\,\mathrm{bei}_2\xi_0\left[M_0 - \frac{ph^2}{8(1 - \nu)}\right]}{h(C + 2\nu G)} \\ C_2 &= \frac{\left(H_0x_0h\frac{\sqrt{2}}{2} - \frac{1}{4}phx_0^2\right)(\xi_0\,\mathrm{bei}_2'\xi_0 + 2\nu\,\mathrm{bei}_2\xi_0) + 2m^2x_0\,\mathrm{ber}_2\xi_0\left[M_0 - \frac{ph^2}{8(1 - \nu)}\right]}{h(C + 2\nu G)} \end{aligned}\right\} \tag{C10}$$

The angle ψ was measured from the junction, and the distance x from the cone apex, as shown in figure 1(b). In equations (C8), (C9), and (C10), ber_2 and bei_2 are Bessel-Kelvin functions of order two, and the primes denote differentiation with respect to ξ. These functions can be changed to order zero by means of recurrence formulas such as those given in reference 5. Then the tables of

these functions appearing in reference 6 can be used to obtain the stresses. Where double signs occur in the equations, the upper sign refers to the inner surface, the lower to the outer surface.

It should be noted that a reasonably accurate determination of discontinuity shear and moment can be made by using the approximate edge-influence coefficients given in references 2 and 7. For a junction of a cone and a portion of a tangent sphere of equal wall thickness and for a cone half-angle of 45°, equations (9c) and (9d) of reference 8 may be reduced to

$$H_0 = \frac{\sqrt{2}ap}{4}\left(1 - \frac{1}{2\lambda}\right) \tag{C11}$$

and

$$M_0 = -\frac{(2 - \nu)a^2p}{16\lambda^3} \tag{C12}$$

REFERENCES

1. Johns, Robert H., and Orange, Thomas W.: Theoretical Elastic Stress Distributions Arising from Discontinuities and Edge Loads in Several Shell-Type Structures. NASA TR R-103, 1961.

2. Timoshenko, S., and Woinowsky-Krieger, S.: Theory of Plates and Shells. Second ed., McGraw-Hill Book Co., Inc., 1959.

3. Hetènyi, M.: Beams on Elastic Foundation. Univ. Mich. Press, 1946.

4. Taylor, Charles E., and Wenk, Edward, Jr.: Analysis of Stress in the Conical Elements of Shell Structures. Rep. 981, David W. Taylor Model Basin, May 1956.

5. Dwight, Herbert Bristol: Tables of Integrals and Other Mathematical Data. Third ed., The Macmillan Co., 1957.

6. Lowell, Herman H.: Tables of the Bessel-Kelvin Functions ber, bei, ker, kei, and Their Derivatives for the Argument Range 0(0.01) 107.50. NASA TR R-32, 1959.

7. Roark, Raymond J.: Formulas for Stress and Strain. Third ed., McGraw-Hill Book Co., Inc., 1954.

8. Johns, Robert H., Morgan, William C., and Spera, David A.: Theoretical and Experimental Analysis of Several Typical Junctions in Space Vehicle Shell Structures. Preprint 2427-62, ARS, 1962.

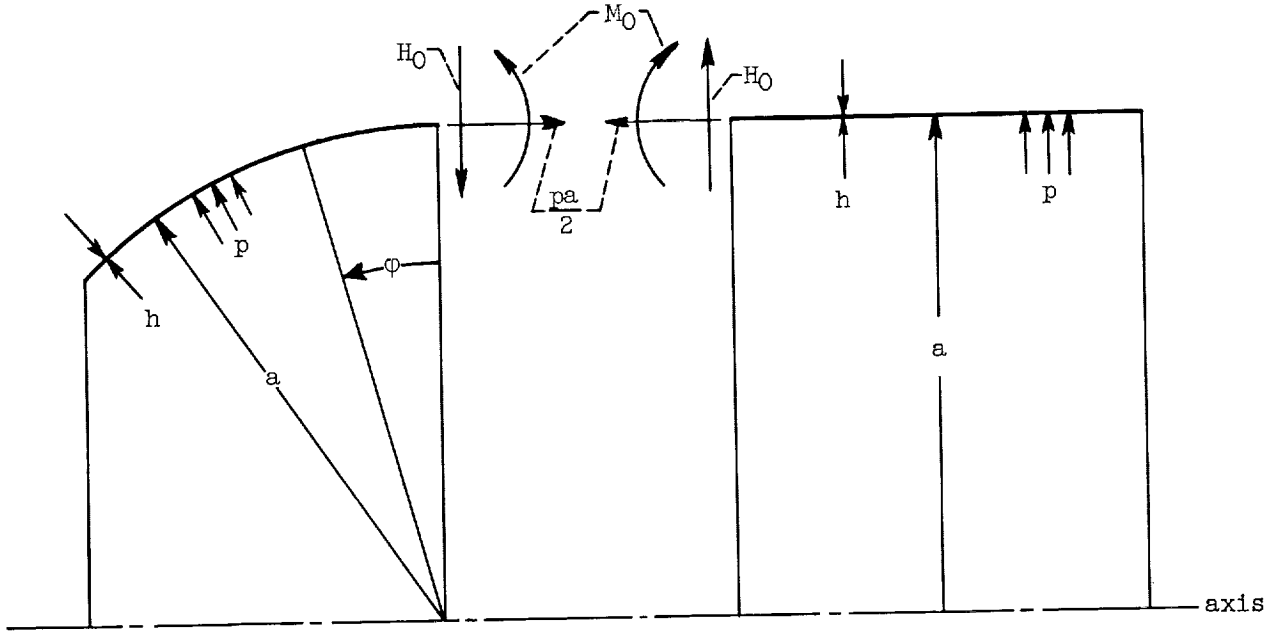

(a) Junction of cylinder and portion of sphere.

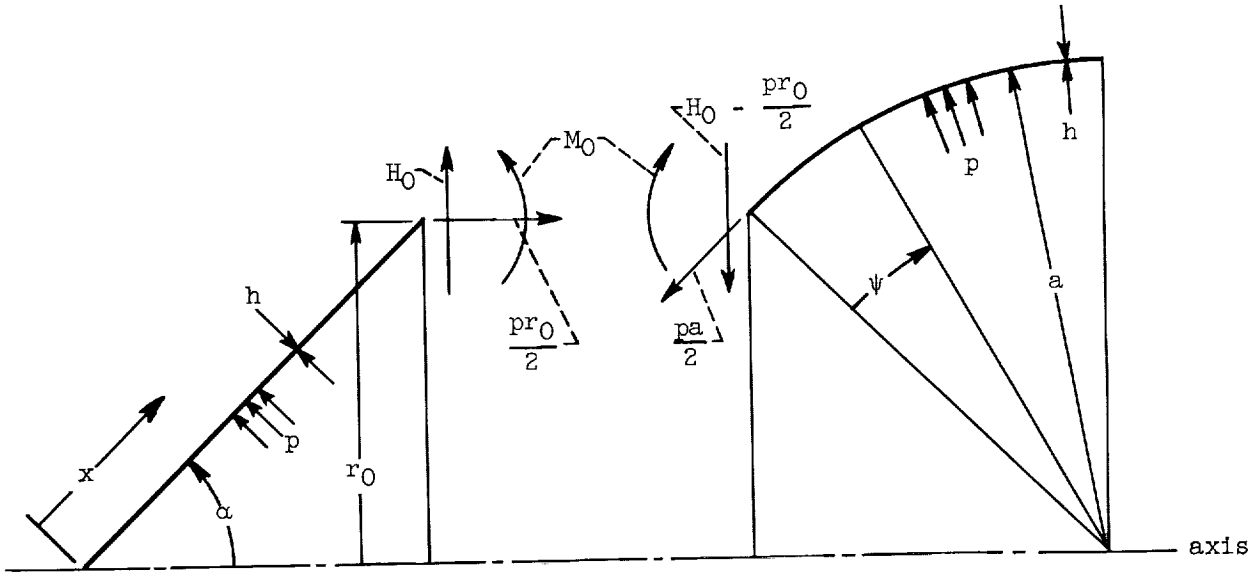

(b) Junction of cone and portion of sphere.

Figure 1. - Geometry and sign convention.

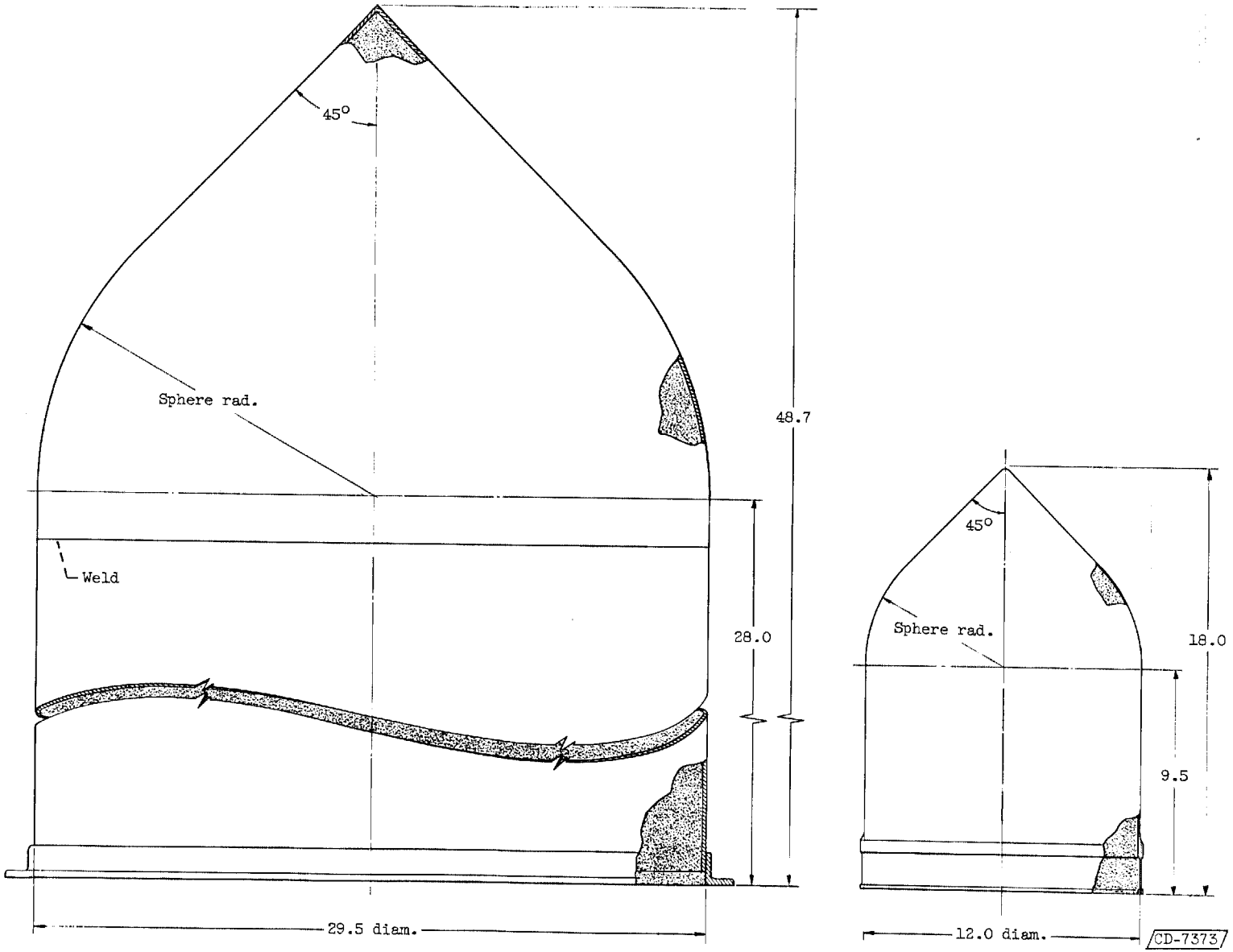

(a) Spun structure.

(b) Machined structure.

Figure 2. - Toriconical structures used in investigation. (Dimensions in inches except where noted.)

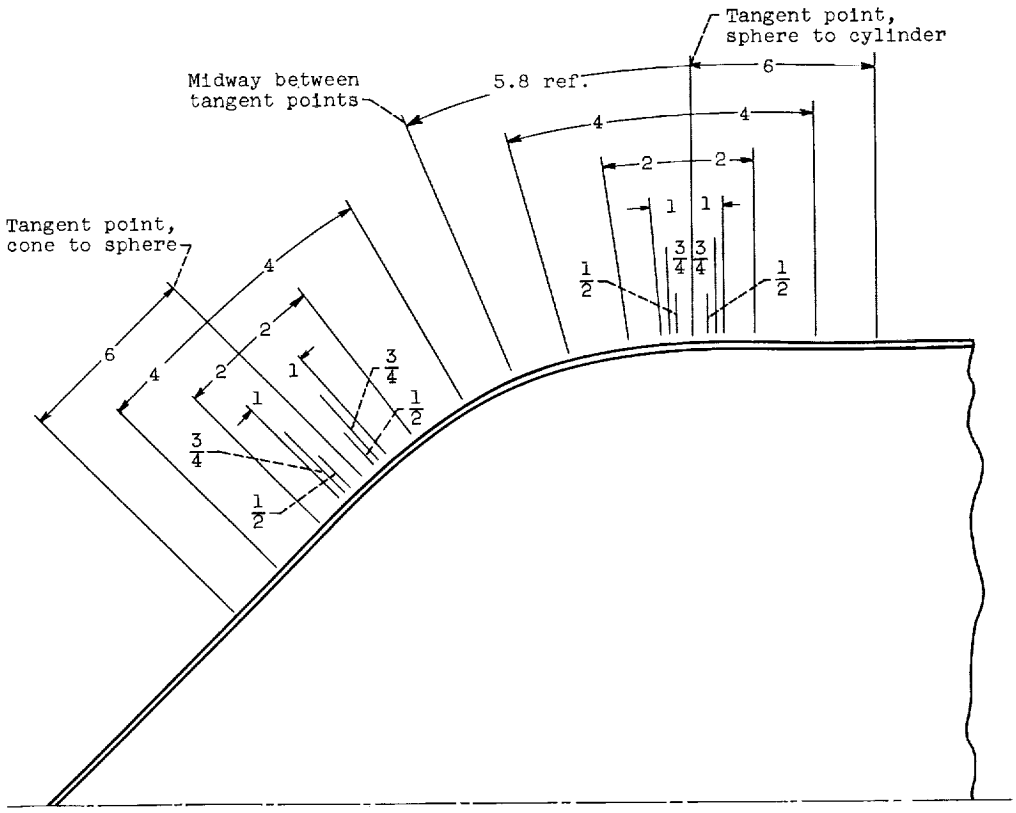

(a) Spun structure.

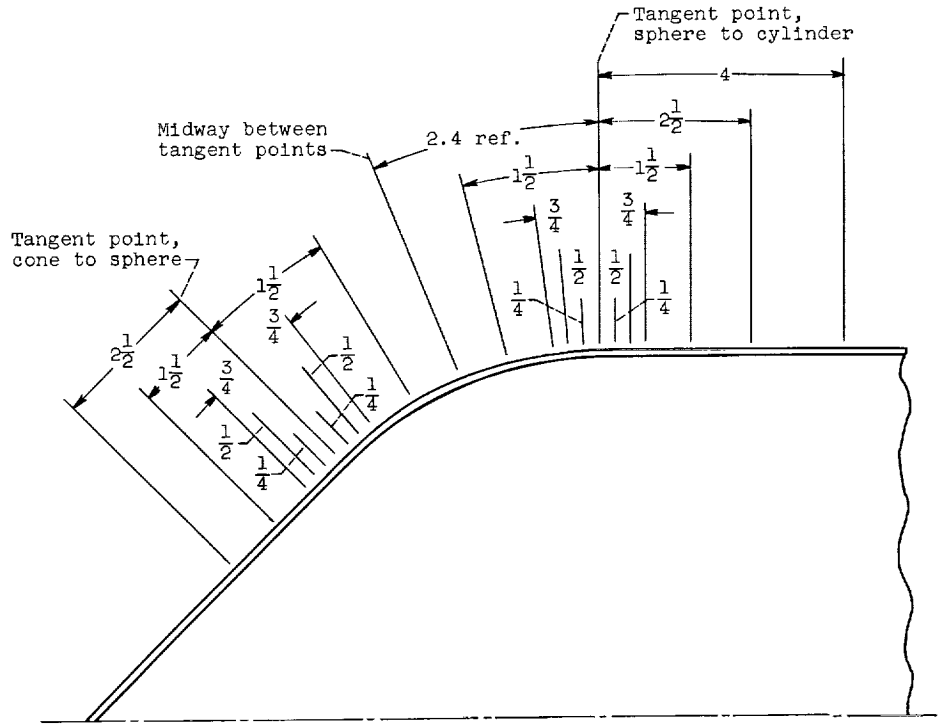

(b) Machined structure.

Figure 3. - Meridional locations of biaxial strain measurements. (Dimensions in inches.)

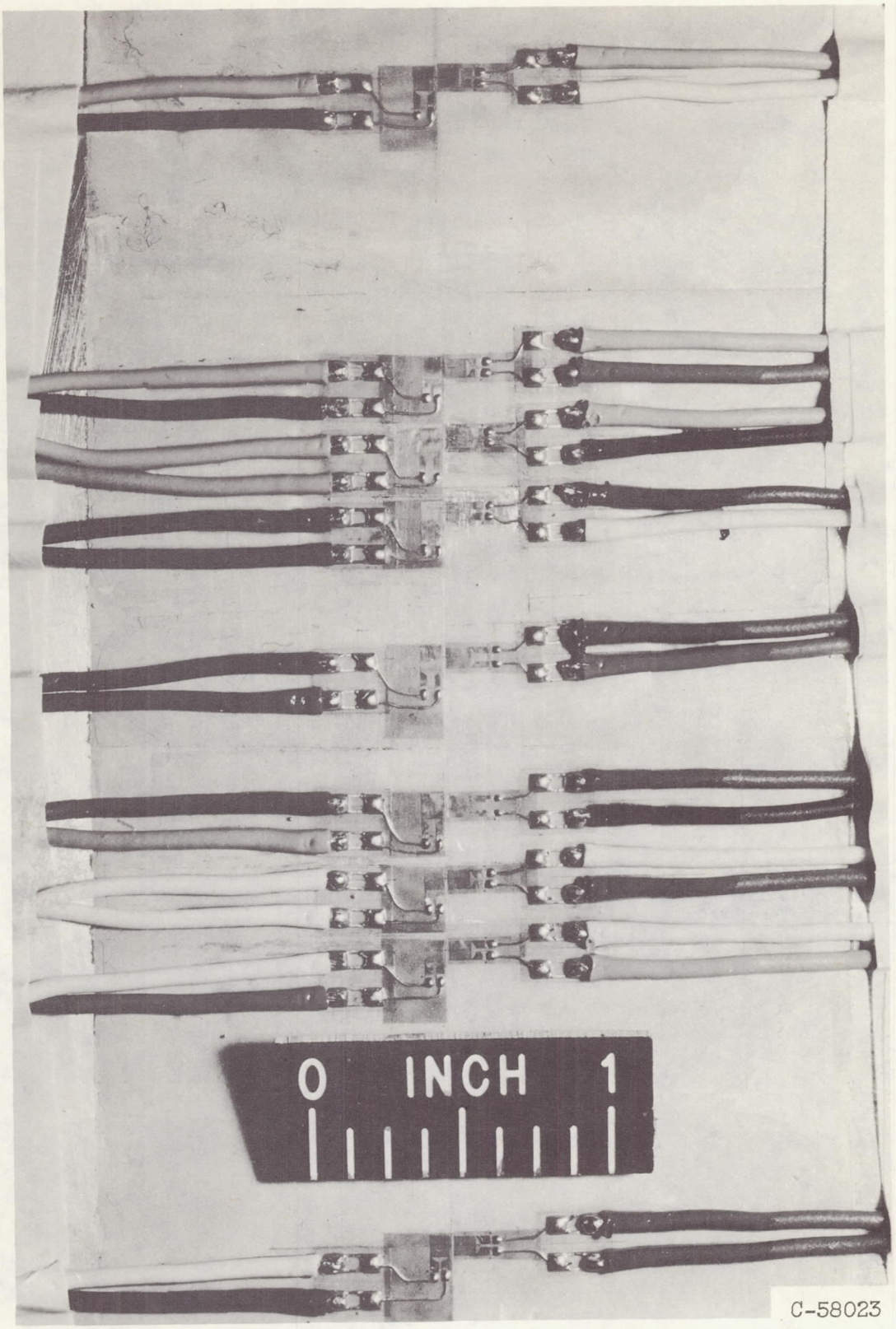

Figure 4. - Gage installation on spun toriconical structure.

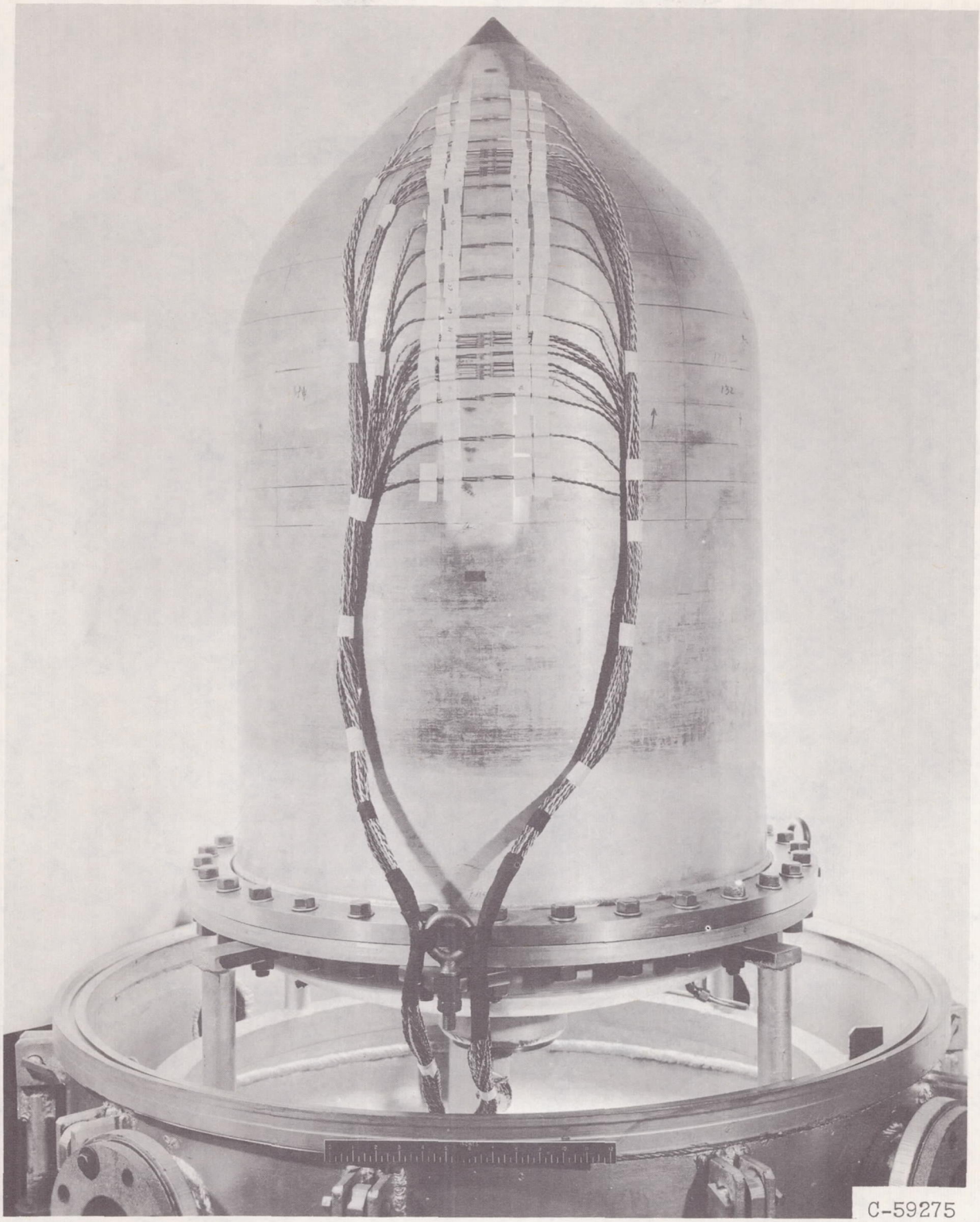

Figure 5. - Spun toriconical structure in test facility.

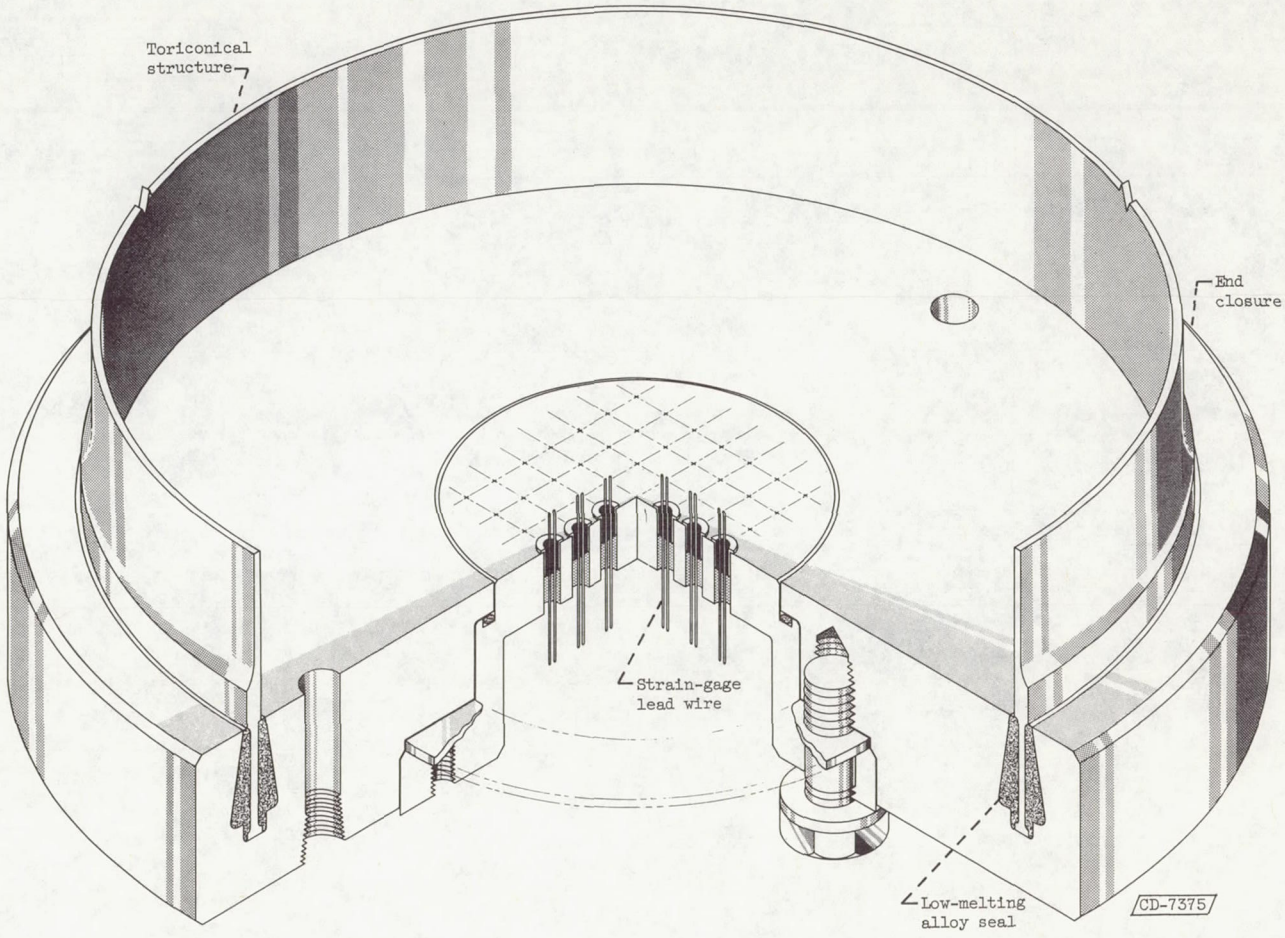

Figure 6. - End closure for machined toriconical structure showing method of bringing out strain-gage lead wire.

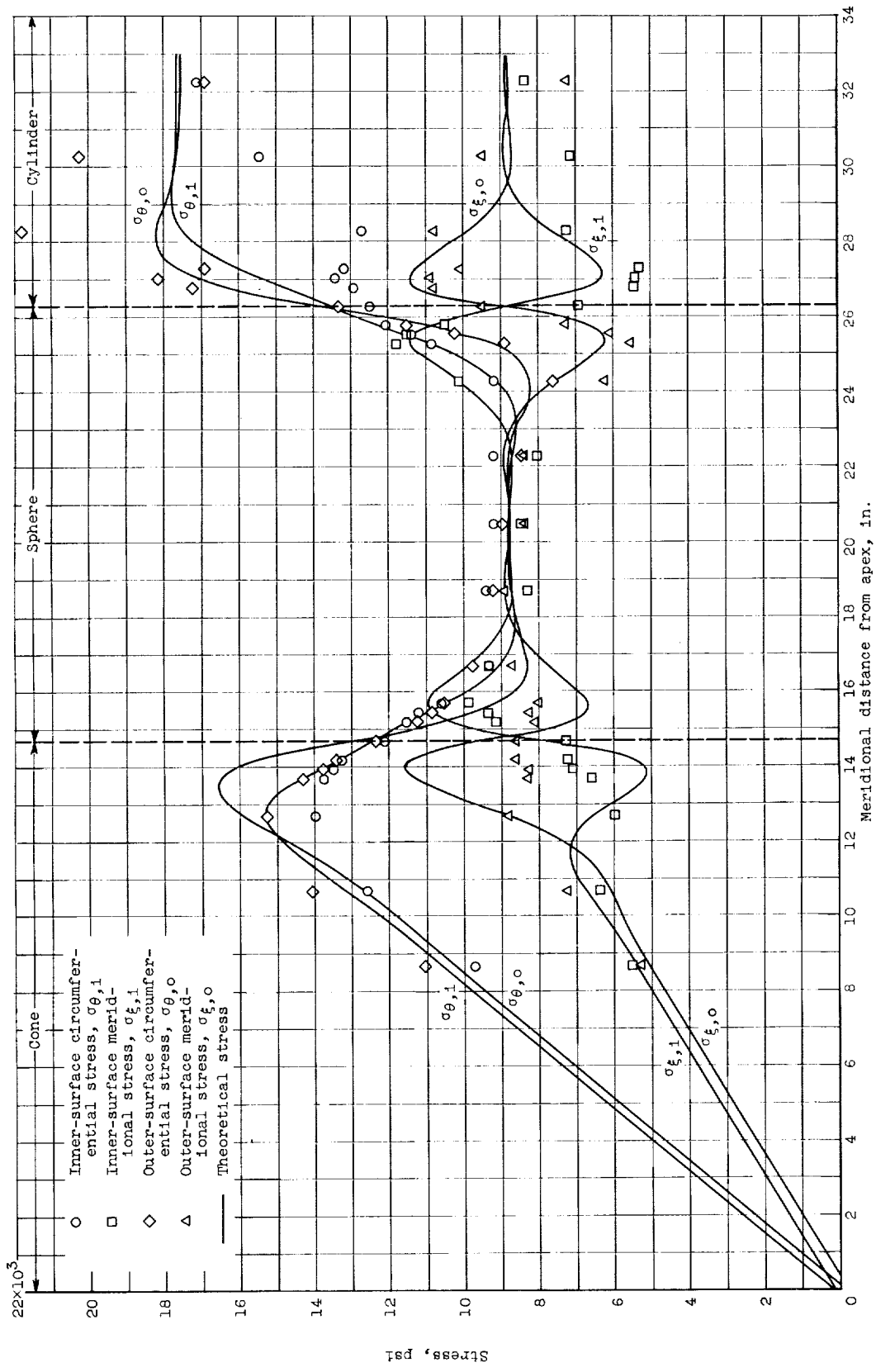

(a) Spun structure; internal pressure, 150 psi.

Figure 7. - Theoretical and experimental principal stresses in toriconical structures.

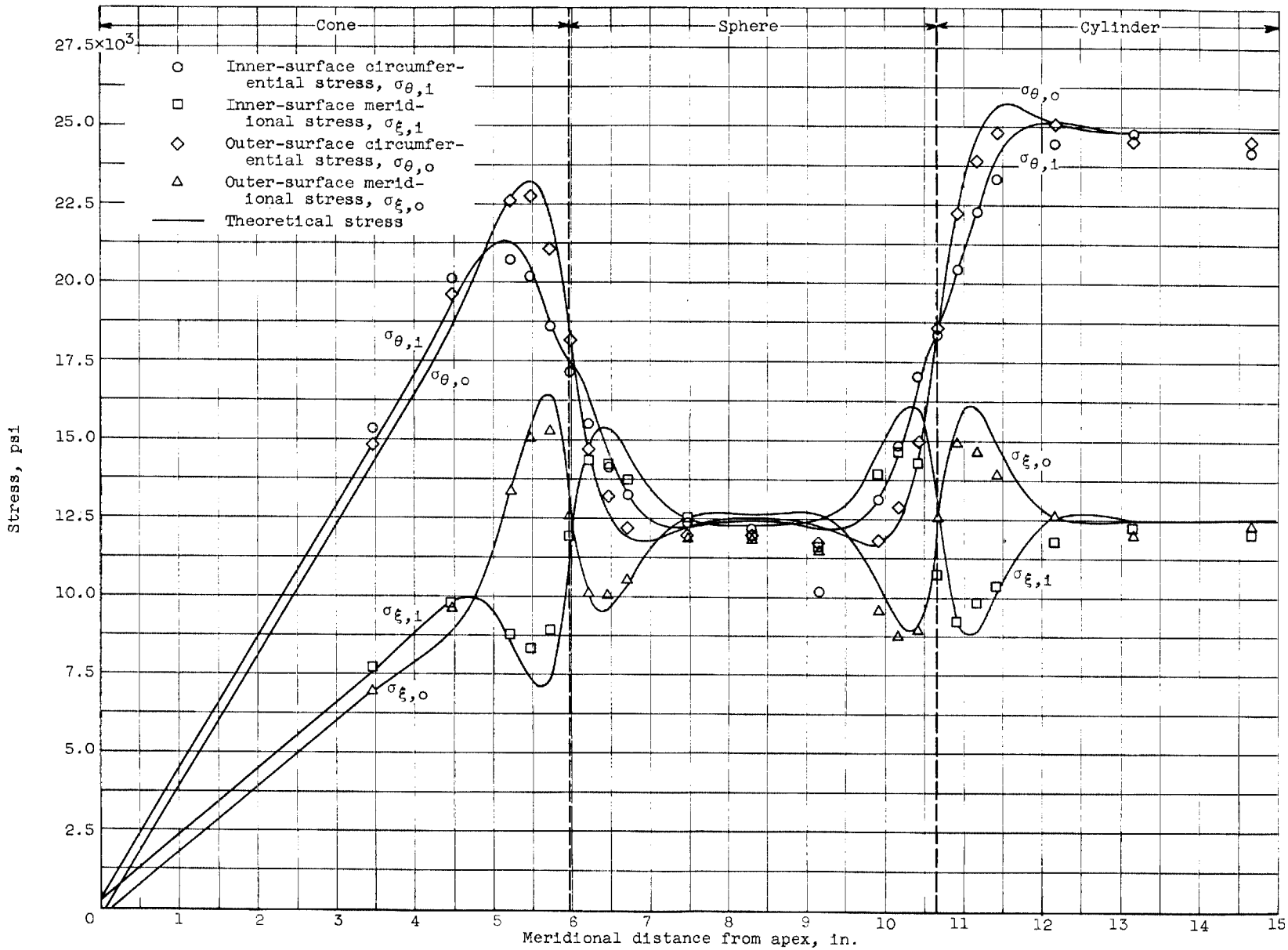

(b) Machined structure; internal pressure, 250 psi.

Figure 7. - Concluded. Theoretical and experimental principal stresses in toriconical structures.

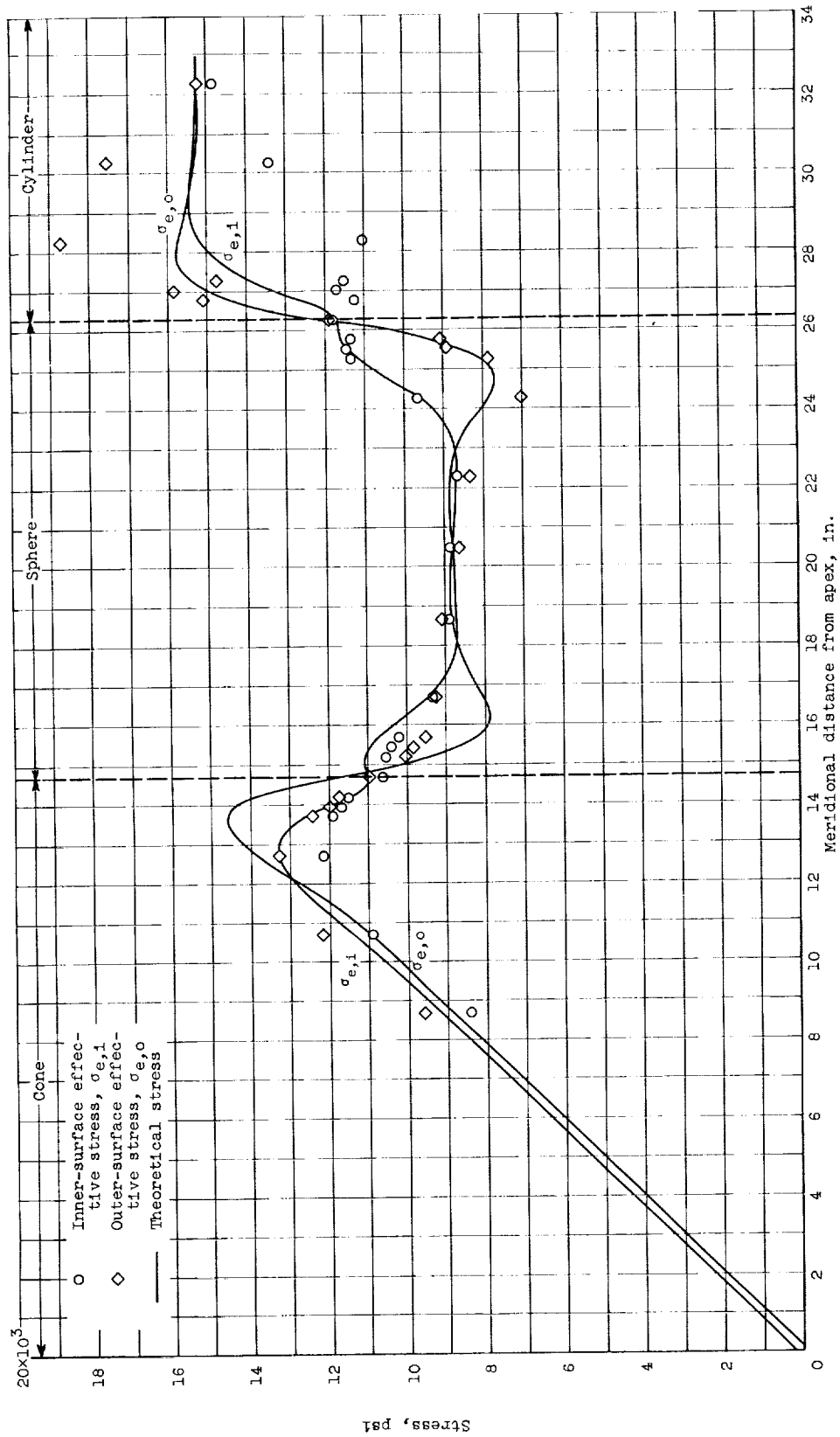

(a) Spun structure; internal pressure, 150 psi.

Figure 8. - Theoretical and experimental effective stresses in toriconical structures.

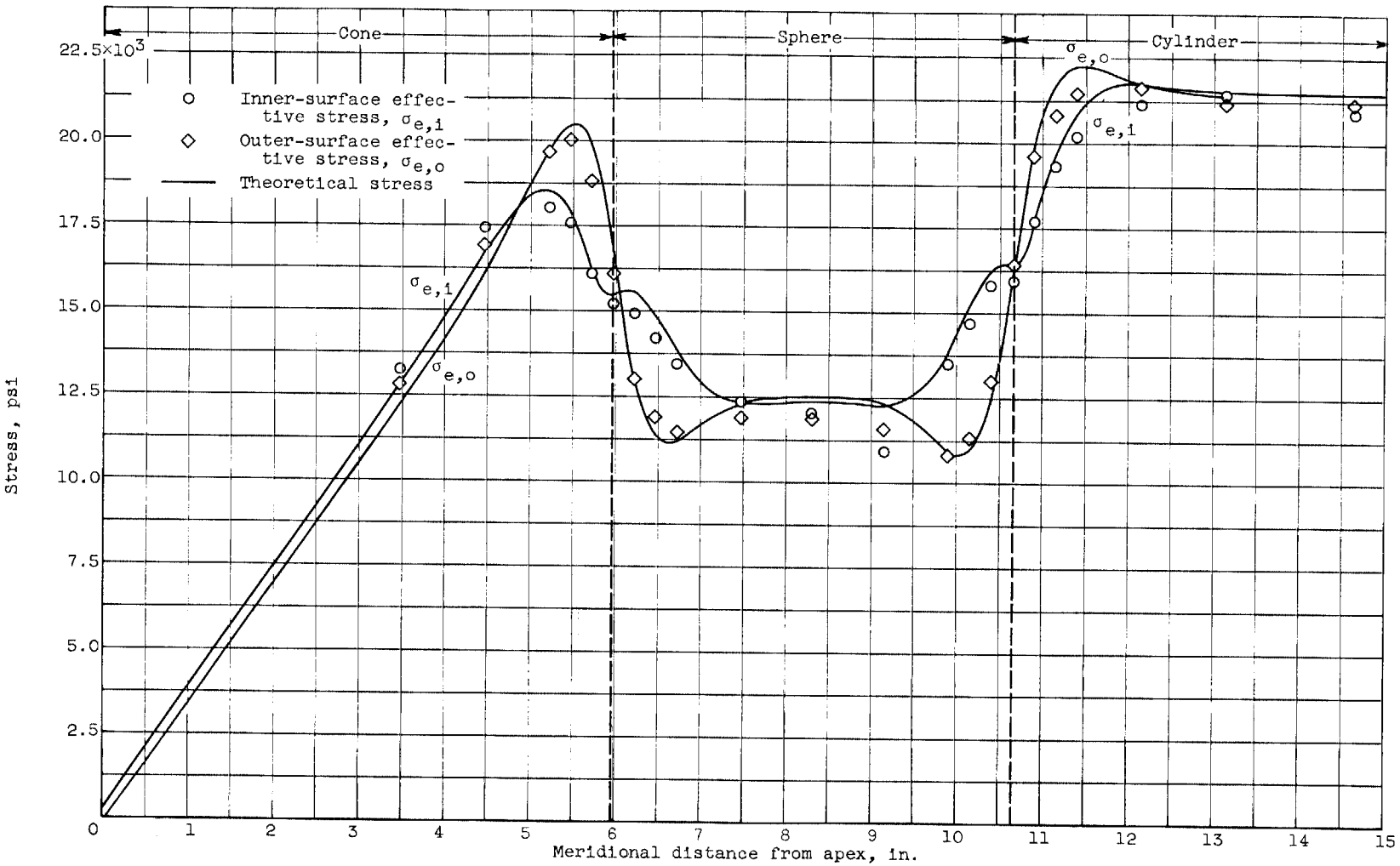

(b) Machined structure; internal pressure, 250 psi.

Figure 8. - Concluded. Theoretical and experimental effective stresses in toriconical structures.

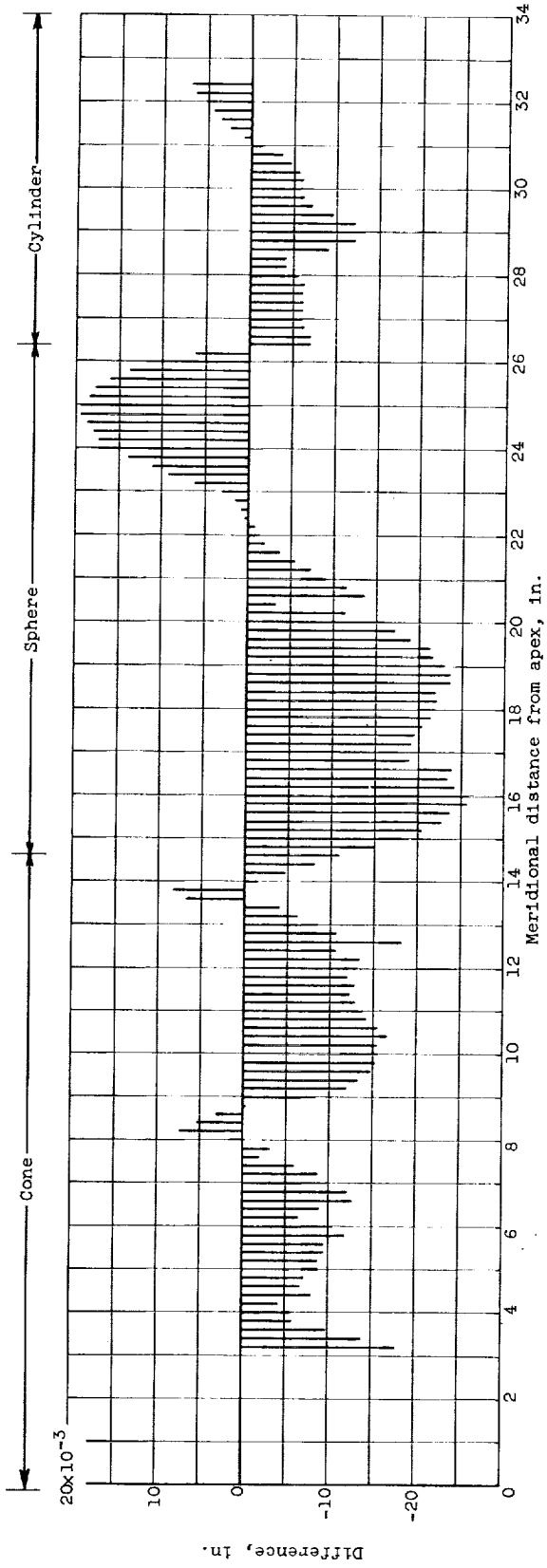

Figure 9. - Difference between theoretical and actual dimensions of spun torisconical structure measured normal to meridian.

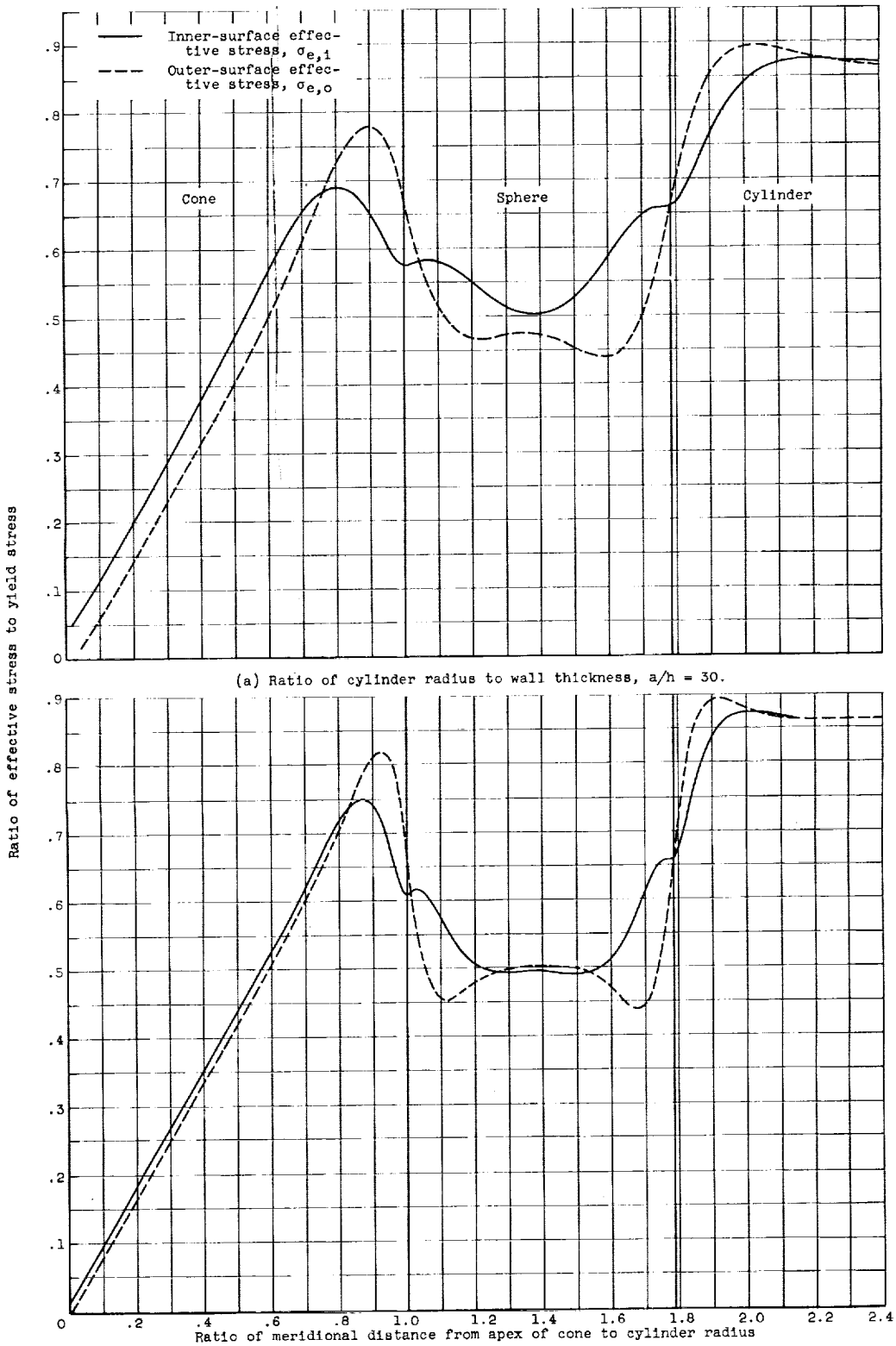

(a) Ratio of cylinder radius to wall thickness, a/h = 30.

(b) Ratio of cylinder radius to wall thickness, a/h = 100.

Figure 10. - Effective stresses for various ratios of cylinder radius to wall thickness. ($E = 10^7$; $\nu = 0.3$)

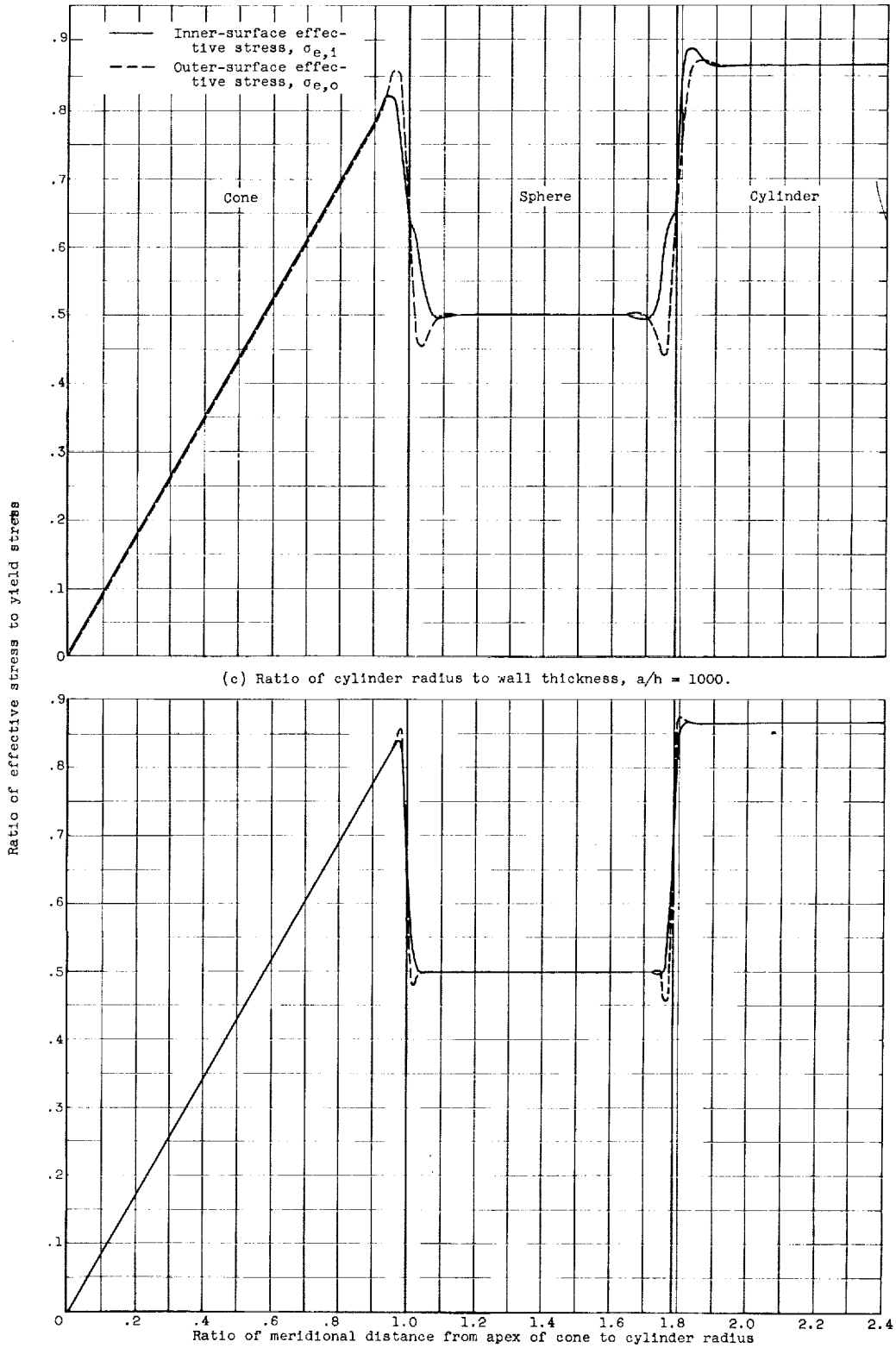

(c) Ratio of cylinder radius to wall thickness, a/h = 1000.

(d) Ratio of cylinder radius to wall thickness, a/h = 10,000.

Figure 10. - Concluded. Effective stresses for various ratios of cylinder radius to wall thickness. ($E = 10^7$; $\nu = 0.3$)